International Journal of Nanoelectronics and Materials
IJNeaM
ISSN 1985-5761 | E-ISSN 2232-1535

Comparison of the Corrosion Behaviour of the Re-cast Aluminium 5083 and Its Bulk Alloy

Zakiah Kamdi[a,b], Loo Yuen Hern[a], Saliza Azlina Osman[a,*], Nur Azam Badarulzaman[a,b] and Tay Sin Kiat[c,d]

[a]*Faculty of Mechanical and Manufacturing Engineering, Universiti Tun Hussein Onn Malaysia, Parit Raja 86400 Batu Pahat, Johor, Malaysia*
[b]*Nanosurf, Faculty of Mechanical and Manufacturing Engineering, Universiti Tun Hussein Onn Malaysia, Parit Raja 86400 Batu Pahat, Johor, Malaysia*
[c]*Intec Precision Engineering Sdn. Bhd., Kawasan Perindustrian Nusa Gemilang, 79200 Iskandar Puteri, Johor, Malaysia*
[d]*AME Manufacturing Sdn. Bhd., Taman Perindustrian Tanjung Pelepas, 81550 Gelang Patah, Johor, Malaysia*
**Corresponding author. Tel.: +607-4537178; fax: +607-4536080; e-mail: salizaz@uthm.edu.my*

ABSTRACT

Aluminium alloys are widely used in various industries due to their excellent properties. In industry, corrosion is always an issue that engineers are mainly concerned. This study will characterise and analyse the corrosion behaviour of the aluminium 5083 bulk alloy, aluminium 5083 machining chip and mixture of aluminium 5083 (bulk alloy and machining chip). The machining chips were melted at 750ºC and re-cast using sand casting. The samples were characterised using Scanning Electron Microscopy (SEM), Energy Dispersive Spectroscopy (EDS), and X-ray diffraction Analysis (XRD). SEM revealed the presence of fusion voids and insoluble phases in the re-cast machining chips. At the same time, EDS identified the presence of oxygen and carbon, indicating the formation of Al_2O_3 and carbides during the sand-casting process. XRD showed peaks corresponding to aluminium magnesium and aluminium silicon. The potentiodynamic polarisation test was performed with a polarisation scan rate of 2 mV/s and a potential range of -1.5 V to 1.5 V, using a saturated Ag/AgCl reference electrode, aluminium samples as the working electrode, and a platinum sheet as the counter electrode. The aluminium 5083 bulk alloy exhibited the lowest corrosion rate (0.88 mm/year), followed by the mixture of aluminium 5083 (bulk alloy and machining chip) (2.15 mm/year), and the aluminium 5083 machining chip (2.93 mm/year). The characterisation of the specimen shows the corrosion product and corrosion pit occur after the corrosion test. These results highlight the superior corrosion resistance of the bulk alloy compared to the machining chip or the mixture.

Keywords: *Aluminium alloy, Machining chips, Casting, Al corrosion, Potentiodynamic polarisation*

1. INTRODUCTION

The rapid development of industrialisation and technological advancements has strongly influenced the utilisation and availability of metals and alloys. Understanding the fundamental theory governing the strengthening behaviour of metals and alloys has expanded significantly over the past few decades, leading to the exploration and development of new alloys. Alloys, which consist of two or more elements, with at least one being a metal, retain the essential properties of metals while often exhibiting additional advantageous characteristics such as increased strength or hardness.

The manufacturing industry relies heavily on alloys to produce objects with specific dimensions and shapes, achieved through various casting processes. However, the corrosion of metals, including alloys, poses a significant challenge in many industries. With its hot and rainy tropical climate, Malaysia provides an ideal environment for corrosion. Corrosion is a destructive chemical attack that can weaken mechanical properties and ultimately lead to structural failure [1]. Aluminium alloys, widely used in various sectors such as renewable energy, electronics, automotive, and aerospace, are susceptible to corrosion under different environmental conditions [2].

In alloy utilisation, machining processes often generate machining chips or swarf as byproducts. The machining of aluminium, a commonly used material, produces these chips, which may have implications for recycling and waste reduction efforts. Furthermore, the behaviour of re-cast alloys formed through casting processes is of interest to understand their corrosion characteristics and compare them to the original alloys.

The Al 5083 has been used commercially due to its excellent resistance to corrosion and high strength-to-weight ratio [3]. However, little research focuses on investigating recycling its machining chip. In addition, the researcher also finds that aluminium suffers substantial corrosion in alkaline solutions [4]. Therefore, this research aims to investigate the corrosion behaviour of aluminium 5083 original alloys, aluminium 5083 machining chip, and a mixture of aluminium 5083 (original alloy and machining chip). The objectives of this study include the characterisation of the surface morphology, microstructure, element composition, and phase analysis of these alloys, as well as comparing their corrosion behaviour. The chosen aluminium alloy, aluminium 5083, known for its favourable properties, will be subjected to sand casting to produce the machining chips and the mixture alloy. The subsequent analyses will involve

scanning electron microscopy (SEM), energy dispersive spectroscopy (EDS), x-ray diffraction (XRD), and electrochemical corrosion test methods, specifically potentiodynamic polarisation and electrochemical impedance spectroscopy (EIS).

By elucidating the corrosion behaviour and comparing the aluminium 5083 original alloy, aluminium 5083 machining chip, and a mixture of aluminium 5083 (original alloy and machining chip), this research aims to provide valuable insights for industries relying on aluminium alloys. Understanding the corrosion resistance and characteristics of these alloys can inform decision-making processes regarding the reuse of machining chips and contribute to waste reduction efforts. Additionally, the findings will deepen the current understanding of the corrosion behaviour of aluminium 5083 original alloys, aluminium 5083 machining chips, and a mixture of aluminium 5083 (original alloy and machining chip), facilitating more informed choices in alloy selection for various applications.

2. METHODOLOGY

The methodology for this study involves several sequential steps to characterise and analyse the corrosion behaviour of the aluminium 5083 original alloy, aluminium 5083 machining chip, and the mixture of aluminium 5083.

The machining chips undergo thorough cleaning to remove any surface contaminants or impurities. Next, the aluminium 5083 machining chip and the mixture of aluminium 5083 undergo melting at a temperature of 750ºC. The molten material is then subjected to sand casting, pouring into mould cavities replicating the desired shapes. The molten material is allowed to cool and solidify, resulting in the formation of re-cast samples. Following the casting process, the samples go through a cutting process to obtain standardised dimensions and shapes. Precise cutting techniques ensure minimal alteration or damage to the sample surfaces.

Once the cutting process is complete, the samples undergo further cleaning to remove any residues or contaminants introduced during cutting. Surface morphology, microstructure, element composition, and phase analysis of the samples are carried out using scanning electron microscopy (SEM), energy dispersive spectroscopy (EDS), and X-ray diffraction (XRD) techniques.

After inspection and qualification, the samples undergo potentiodynamic polarisation tests and electrochemical impedance spectroscopy (EIS). Potentiodynamic polarisation tests sweep the potential from -1.5 V vs OCP to +1.5 V vs OCP in 0.5M NaOH at a scan rate of 0.002 V/s. EIS is performed within a frequency range of 0.01 Hz to 10 kHz and an amplitude of 0.005 VRMS. Post-corrosion tests, the samples are subjected to SEM, XRD, and EDS analysis to assess any changes in surface morphology, phase composition, and elemental composition caused by corrosion. The obtained data from the corrosion tests, including polarisation curves and impedance spectra, are analysed to compare the corrosion behaviour of all samples. The results are interpreted, conclusions are drawn, and the implications of the findings are discussed.

2.1 Material

Aluminium 5083 is the raw material selected for this study. The chemical composition of aluminium 5083 is given in Table 1. In this study, the three samples are the aluminium 5083 original alloy, the aluminium 5083 machining chip, and a mixture of aluminium 5083 (original alloy and machining chip). Table 2 shows the material designation for these three samples.
The bulk material and machining chips were degreased in an ultrasonic bath filled with acetone for 30 minutes. This process effectively removes any grease, coolant, or other contaminants present on the surface of the bulk material and machining chips. Subsequently, thorough rinsing in deionised water is performed to eliminate any remaining residues. Finally, the samples are carefully dried under sunlight to ensure complete moisture evaporation.

Table 1 Chemical Composition of Aluminium 5083

Element	Cr	Cu	Fe	Mg	Mn	Si	Ti	Zn	Al
Percentage	0.05-0.25	0.1	0.4	4.0-4.9	0.4-1.0	0.4	0.15	0.25	Balance

Table 2 Material Designation for Samples

Material Designation	**Material Composition (wt%)**	
	Al 5083 Original Alloy	**Al 5083 Machining Chip**
Al 5083_A	100	0
Al 5083_B	0	100
Al 5083_C	75	15

2.2 Sand Casting

The sand casting process in this study focuses specifically on Al 5083_B and Al 5083_C samples. A wooden mould pattern with dimensions of 200 mm × 1000 mm × 10 mm is produced. This mould pattern serves as the template for the sand-casting process. After the mould pattern is prepared, the casting sand, known as Green Sand, is meticulously crafted. Green Sand is composed of silica sand, clay, and water. The clay acts as a binder, while the water provides moisture to the Green Sand mixture. The specific composition of the Green Sand is detailed in Table 3.

Table 3 Composition of Green Sand

Material	Silica Sand	Clay	Water
Composition (wt%)	70	20	10

Once the mould pattern and Green Sand are ready, the drag mould is created using a Jolt & Squeeze Molding Machine. This machine produces both the cope and drag moulds necessary for sand-casting. Next, the machining chips are melted in a crucible furnace at a temperature of 750°C. The molten aluminium alloy is then cooled to the desired pouring temperature at 650°C for aluminium alloys. The molten alloy is poured into the mould and left to solidify. After solidification, the workpiece is removed from the mould and allowed to cool at room temperature. To facilitate the visualisation of the process, Figure 1(a) showcases the crucible furnace, while Figure 1(b) illustrates the cope and drag mould.

Figure 1. (a) Crucible Furnace (b) Cope and Drag Mould.

2.3 Specimen Preparation

The cutting process involves three specimens: Al 5083_A, Al 5083_B, and Al 5083_C. These samples undergo cutting using three distinct machines: the Fully Auto-Bandsaw, the Milling Machine Bed type, and the EDM Wire Cut. The wire-cut process is specifically used to achieve the desired dimensions for the samples required for the potentiodynamic polarisation test. Prior to initiating the cutting process, a design drawing of the workpiece must be created. This design drawing is generated using AutoCAD 2022 software. The specified dimensions for the workpiece are 10 mm × 10 mm × 5 mm. The surfaces of the samples were mechanically polished with silicon carbide papers (Grade numbers 400, 600, 800, 1000, 1200, 2000, and 2500). After the metallographic polishing, the test specimens were deoiled using acetone and then washed with deionised water and absolute alcohol to remove any remaining residues.

2.4 Surface Morphology and Elemental Analysis

The surface morphology of Al 5083_A, Al 5083_B, and Al 5083_C that undergo corrosion test were compared with the un-corroded Al 5083_A, Al 5083_B, and Al 5083_C by capturing the SEM Images with x500 SE and x2.00k SE using the Hitachi Scanning Electron Machine. The energy dispersive x-ray (EDS) analysis was also carried out for corroded and un-corroded Al 5083_A, Al 5083_B, and Al 5083_C.

2.5 Phase Analysis

The corroded and un-corroded Al 5083_A, Al 5083_B, and Al 5083_C phase analysis was done using the D8-Advance Bruker XRD Machine. The graph obtained will be analysed by using the analysis software. The XRD analysis was scanned at 5^0/min, with step size 0.02^o from 20^o to 85^o.

2.6 Specimen Preparation for Corrosion Test

To prepare the test samples for further analysis, the specimens with dimensions of 10 mm × 10 mm × 5 mm are mounted in epoxy resin, leaving an exposed area of 1 cm2 for interaction with the electrolyte solution. Subsequently, the cross-section of the mounted samples is carefully polished using a series of silicon carbide papers with different grades (400, 600, 800, 1000, 1200, 2000, and 2500). This polishing procedure ensures a smooth and uniform surface, which is essential for accurate

measurements and observations. Furthermore, the coated test specimens must be securely welded with a wire to facilitate current flow during the Potentiodynamic Polarization Test.

2.7 Alkaline Electrolyte

To create standard solutions of sodium hydroxide, analytical-grade sodium hydroxide pellets were dissolved in distilled water. A total of 20 grams of sodium hydroxide pellets were dissolved in 1000 ml of distilled water, producing a 0.5M NaOH solution.

2.8 Potentiodynamic Polarisation Test

Three experiments involved Al 5083_A, Al 5083_B, and Al 5083_C were immersed in a 0.5M NaOH solution. A three-electrode cell was utilised as the electrode system for the potentiodynamic polarisation test. The reference electrode (RE) was made of Silver Chloride (AgCl), the counter electrode (CE) was a platinum sheet, and the working electrode was an aluminium alloy. These electrodes were connected to a potentiostat, which was then linked to a computer for data acquisition. The test specimen had an exposed surface area of 1cm2, and the potentiodynamic polarisation test was conducted at a scan rate of 2 millivolts per second. The potential range for the test was set from -1.5 V to +1.5 V, and the experiments were carried out at ambient room temperatures, typically ranging from approximately 21℃ to 25℃. Upon completion of the test, the system generated a polarisation curve graph. The graph was reproduced in the Origin Lan 2019 software to analyse the data, and the values of E_{corr} (corrosion potential), i_{corr} (corrosion current) and corrosion rate were obtained.

2.9 Electrochemical Impedance Spectroscopy (EIS)

This research involves three experiments using three different types of specimens: Al 5083_A, Al 5083_B, and Al 5083_C immersed in 0.5M NaOH solution. These experiments' experimental setup and conditions are identical to those of the Potentiodynamic Polarization Test described earlier. In addition to the Potentiodynamic Polarization Test, Electrochemical Impedance Spectroscopy (EIS) is performed in this study. The EIS measurements are conducted over a frequency range from 0.01 Hz to 10 kHz, with an applied amplitude of 0.005 V^{RMS}.

3. RESULTS AND DISCUSSION

3.1 Surface Morphology, Microstructure and Element Composition Analysis Before Test

Figure 2 illustrates magnified images of Al 5083_A, Al 5083_B, and Al 5083_C captured using a Scanning Electron Microscope (SEM). The figure includes two magnification levels, x500 and x2.00k, which provide detailed views of the ground aluminium alloy substrate. In Figure 2 (a & b), the images reveal the presence of both smooth areas and visible grinding scratches on the specimens. These surface features indicate the effects of the grinding and polishing process. In Figure 2 (c - f), important characteristics such as fusion voids and insoluble phases can be observed in the Al 5083_B and Al 5083_C specimens. Fusion voids are detected, indicating areas where incomplete fusion occurred during machining. The formation of voids is due to the precipitation of hydrogen (known to have a high solubility in aluminium) in a molecular form on the surface [5]. These voids raise concerns regarding the structural integrity and performance of the material. Additionally, insoluble phases are identified within the images, indicating the presence of certain alloy constituents that remain in an insoluble state [6].

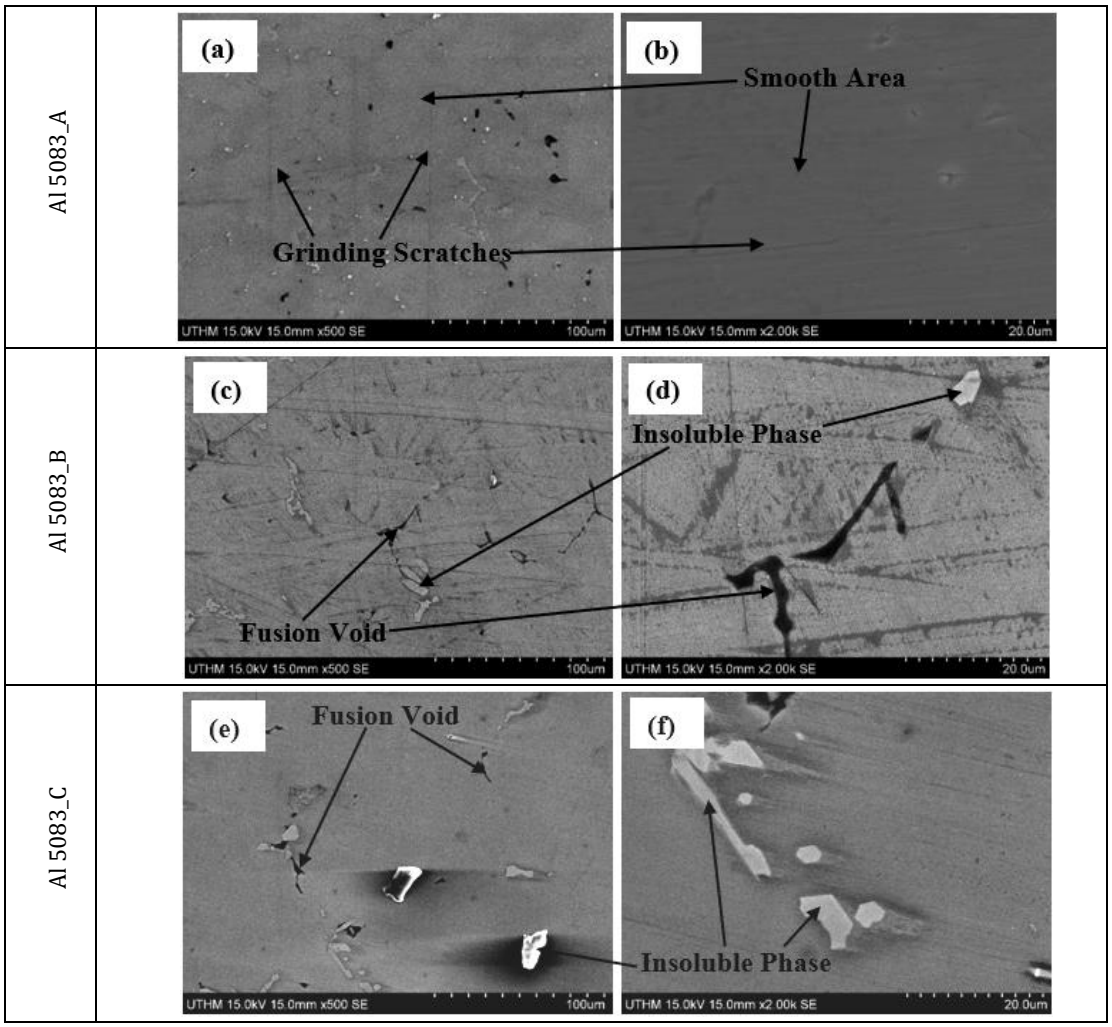

Figure 2. SEM Surface Morphology of Al samples before test at (a, c & e) X 500 and (b, d & f) 2.00k magnification.

Table 4 shows the elemental distribution in Al 5083_A, Al 5083_B, and Al 5083_C. In Al 5083_A, the EDS analysis in Table 4 reveals a weight percentage of 95.16 wt% for aluminium (Al) and 4.84 wt% for magnesium (Mg), confirming the expected composition of aluminium 5083. For Al 5083_B, the element distribution analysis shows weight percentages of 95.20 wt% for aluminium and 4.80 wt% for magnesium. For Al 5083_C, the results show a weight percentage of 95.16 wt% for aluminium and 4.84 wt% for magnesium. A notable difference can be observed in the weight percentage of aluminium between Al 5083_B and Al 5083_C. This discrepancy arises because Al 5083_B involved only melted machining chips, whereas Al 5083_C included a mixture of 75% original alloy and 15% machining chips.

Table 4 EDS analysis for Al 5083_A, Al 5083_B and Al 5083_C

	Elemental Composition	Weight Percentage (%)
Al 5083_A	Magnesium	4.84
	Aluminium	95.16
Al 5083_B	Magnesium	4.80
	Aluminium	95.20
Al 5083_C	Magnesium	4.84
	Aluminium	95.16

3.2 Phase Analysis

Figure 3 (a–c) displays the X-ray diffraction (XRD) analysis results conducted on Al 5083_A, Al 5083_B, and Al 5083_C. The XRD patterns show well-defined and sharp peaks. In Figure 3 (a), the main peaks correspond to aluminium magnesium and aluminium silicon, with 2 Theta angle intensities at (38.40º, 44.80º, 60.90º, 77.80º, 82.00º). Similarly, Figure 3 (b) exhibits main peaks associated with aluminium magnesium and aluminium silicon, displaying 2 Theta angle intensities at (38.30º, 44.80º, 60.90º, 77.90º, 82.00º). Figure 3 (c) also reveals the main peaks of

aluminium magnesium and aluminium silicon, with 2 Theta angle intensities at (38.40º, 44.70º, 60.90º, 77.80º, 82.00º). Comparing the XRD graphs, it is evident that the main peaks observed in each sample are nearly identical, and the patterns of 2 Theta angle intensities show similarities.

3.3 Potentiodynamic Polarization Test Analysis

The corrosion behaviour of Al 5083 aluminium alloy samples (Al 5083_A, Al 5083_B, and Al 5083_C) in a 0.5 M NaOH solution was analysed. Table 5 revealed that Al 5083_B exhibited the highest corrosion current density (i_{corr}) and corrosion rate, while Al 5083_A demonstrated the lowest values, indicating superior corrosion resistance. The corrosion rate values followed a similar trend to the corrosion current density, with lower corrosion current density corresponding to a lower corrosion rate. Additionally, Al 5083_B exhibited the highest E_{corr}, indicating decreased corrosion resistance, while Al 5083_A had the lowest E_{corr}. Calculating the corrosion rate using i_{corr} showed that Al 5083_A displayed the highest corrosion resistance (0.8801 mm/year), followed by Al 5083_C (original alloy & machining chip) (2.1470 mm/year), and Al 5083_B (2.9341 mm/year). The controlled microstructure of the original aluminium alloy contributed to its enhanced corrosion resistance, while the altered microstructure of re-cast machining chips increased its susceptibility to corrosion.

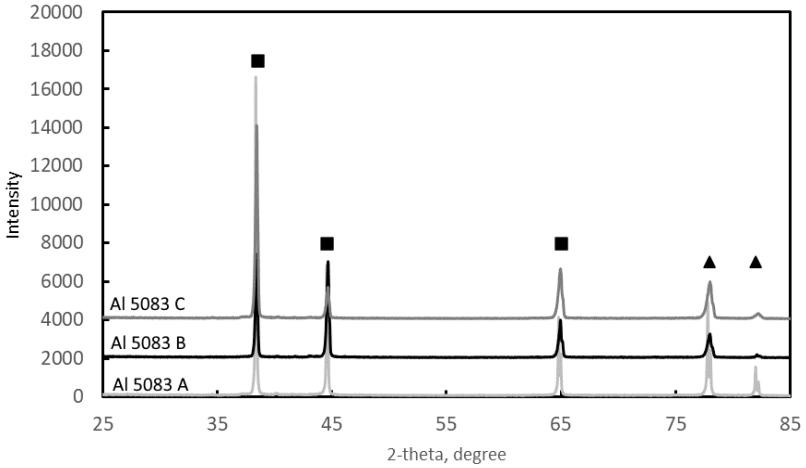

Figure 3. XRD Analysis Graph of Samples (a) Al 5083_A (b) Al 5083_B (c) Al 5083_C.

Figure 4 presented the polarisation curve of the three samples in a 0.5 M NaOH solution, showing the initial stages of corrosion. The figure illustrated the passivation behaviour of aluminium, primarily attributed to the formation of corrosion products such as Al_2O_3 and $Al(OH)_3$ when aluminium reacts with water. The corrosion products formed two distinct phases, with $Al(OH)_3$ initially being gelatinous and gradually transforming into more stable Al_2O_3. Aluminium has inherent passivating properties, and creating an Al_2O_3 passivating film on the surface contributed to its corrosion resistance.

Table 5 Polarization result for Al 5083_A, Al 5083_B and Al 5083_C in 0.5M NaOH

Aluminium 5083 Samples	E_{corr} Obs (V)	I_{corr} (A/cm2)	Polarisation resistance (Ω)	Corrosion Rate (mm/year)
Al 5083_A	-1.4283	7.1002 x10-5	14.04	0.8204
	-1.4342	8.087 x10-5	16.284	0.9397
Al 5083_B	-1.3976	25.366 x10-5	16.776	2.9475
	-1.4223	25. x10-5	17.072	2.9206
AL 5083_C	-1.4236	18.785 x10-5	10.457	2.1828
	-1.4253	18.169 x10-5	11.415	2.1112

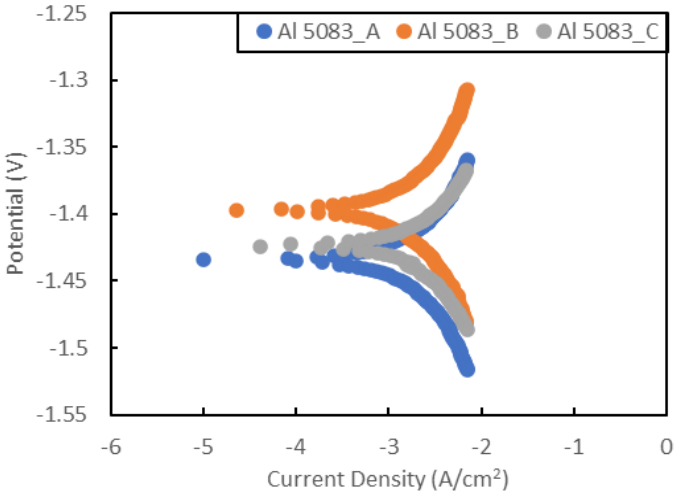

Figure 4. Polarization Curve of Al 5083_A, Al5083_B and Al5083_C.

When Al 5083 samples are exposed to 0.5 M NaOH, a protective film of alumina forms on their surfaces due to the reaction of aluminium with air. However, due to chemical dissolution, this alumina layer quickly dissolves when immersed in 0.5 M NaOH [7]. The main cathodic reaction is the reduction of water:

$$2H_2O + 2e^- \rightarrow H_2(g) + 2OH^-(aq) \quad (1)$$

The reduction of water leads to hydroxide ions (OH-) formation and an increase in pH at the film/solution interface. This localised increase in pH accelerates the corrosion reaction and damages the passive film. The anodic dissolution of aluminium in alkaline mediums occurs through the addition of surface hydroxyl species, ultimately resulting in the chemical dissolution of $Al(OH)_3$ in the presence of the surface oxide film. This anodic reaction contributes to the overall corrosion of aluminium in alkaline solutions represented under:

$$Al + 4OH^- \rightarrow Al(OH)^- + 3e^- \quad (2)$$

The main reaction can be represented as

$$2Al + 2OH^- + 6H_2O \rightarrow 2Al(OH)^{4-} + 3H_2 \quad (3)$$

3.4 Electrochemical Impedance Spectroscopy Analysis

Electrochemical impedance spectroscopy (EIS) was used to evaluate the corrosion resistance of the film layer on Al 5083_A, Al 5083_B and Al 5083_C in a 0.5 M NaOH electrolyte. Figure 5 shows the EIS data in the form of a Nyquist plot. The appearance of the inductive loop is due to the occurrence of adsorbed intermediate on the surface by AL^{2+} or Al^{3+} [9]. In the Nyquist plot, the curve for Al 5083_A is positioned at a higher frequency than that of Al 5083_C, and Al 5083_C exhibits a higher frequency curve than Al 5083_B. This indicates that higher curves correspond to more excellent corrosion resistance and lower charge generation on the sample's surface. The results from Figure 6a are consistent with the data in Table 5, supporting the reliability of the findings.

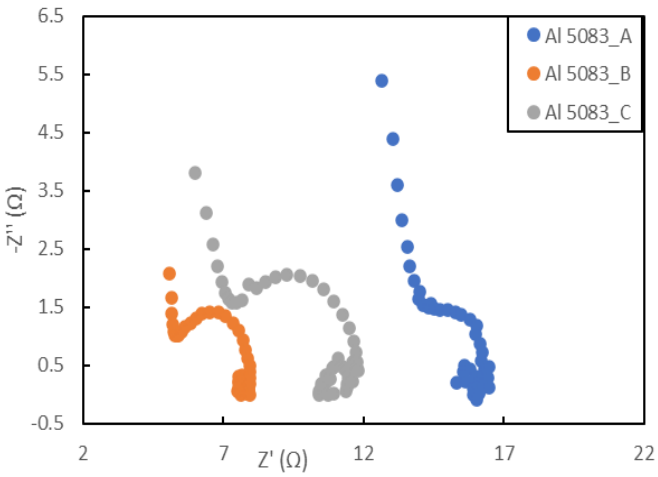

Figure 5. Comparison of EIS Spectra of Different Samples Nyquist Plots.

3.5 Surface Morphology, Microstructure and Element Composition Analysis After Corrosion Test

The surface morphology and microstructure of Al 5083_A, Al 5083_B, and Al 5083_C were analysed using a Scanning Electron Microscope (SEM) after the Potentiodynamic Polarization Test. Figure 6 shows the samples' magnified secondary electron SEM images (x500 and x2.00k). A notable difference can be observed when comparing Figure 2 to Figure 6. In Figure 6 (a - f), the presence of a corrosion product (white substrate) are visible, while these features are not observed in Figure 2 (a-f). One noteworthy observation is the formation of a corrosion product, indicating areas where the aluminium (Al) has undergone oxidation, producing Al_2O_3 [10].

The analysis of element distribution using Energy Dispersive Spectroscopy (EDS) in conjunction with a Scanning Electron Microscope (SEM) was performed on the samples Al 5083_A, Al 5083_B, and Al 5083_C after the corrosion test. Table 6 provides the results of the EDS analysis. For Al 5083_A, the analysis revealed significant amounts of oxygen (O) at 50.93 wt%, followed by aluminium (Al) at 28.83 wt%, and carbon (C) at 12.91 wt%. Smaller quantities of other elements were also present. The oxygen weight percentage was higher than other elements, indicating the accumulation of corrosion products on the sample's surface.

In the case of Al 5083_B, the EDS analysis showed significant amounts of oxygen (O) and aluminium (Al) in the spectra, confirming the presence of corrosion products. The weight percentage of oxygen was the highest, followed by aluminium and magnesium (Mg). For Al 5083_C, the EDS analysis revealed varying weight percentages of oxygen, aluminium, magnesium, and carbon across the spectra, indicating different amounts of corrosion products and surface characteristics of the original alloy, machining chip, and their combination. Overall, the EDS analysis provided insights into the elemental composition and distribution on the surface of the samples, confirming the presence of corrosion products and highlighting the differences between the samples.

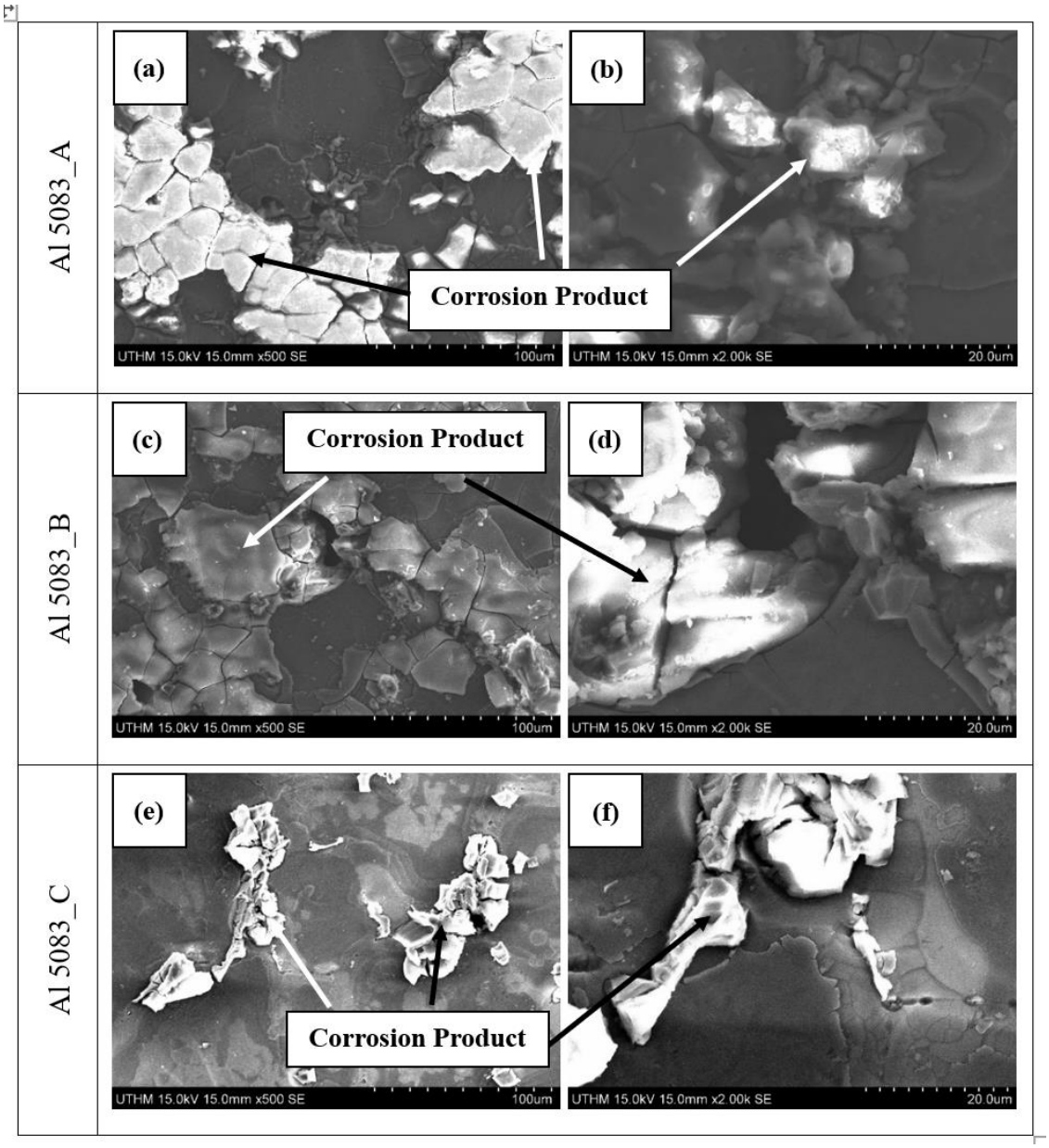

Figure 6. SEM Surface Morphology of Al samples after test at (a, c & e) X 500 and (b, d & f) 2.00k magnification.

Table 6 EDS analysis After Corrosion Test of Al 5083_A, Al 5083_B and Al 5083_C

	Elemental Composition	**Weight Percentage (%)**		**Elemental Composition**	**Weight Percentage (%)**
Al 5083_A	Carbon	12.91	**Al 5083_C**	Carbon	10.44
	Oxygen	50.93		Oxygen	20.28
	Sodium	0.44		Magnesium	4.94
	Magnesium	5.62		Aluminium	64.34
	Aluminium	28.83			
	Silicon	0.16			
	Manganese	0.65			
	Iron	0.47			
Al 5083_B	Carbon	12.15			
	Oxygen	49.51			
	Magnesium	6.71			
	Aluminium	31.63			

4. CONCLUSION

In conclusion, the study successfully characterised the aluminium 5083 original alloy, aluminium 5083 machining chip, and the mixture of aluminium 5083 using SEM, EDS, and XRD analyses. Fusion voids and insoluble phases were observed in the SEM results, indicating incomplete fusion and potential impurities. EDS analysis revealed the presence of oxygen and carbon, indicating oxidation and amorphous organic substances. XRD analysis identified main peaks corresponding to aluminium magnesium and aluminium silicon.

The corrosion behaviour of the three samples was compared using a potentiodynamic polarisation test. The aluminium 5083 original alloys exhibited the lowest corrosion rate, indicating the highest corrosion resistance. The aluminium 5083 machining chip had the highest corrosion rate and lowest resistance, while the mixture of aluminium 5083 showed an intermediate corrosion rate. Based on these findings, it can be concluded that the aluminium 5083 original alloy has the highest corrosion resistance, followed by the mixture, and the machining chip has the lowest resistance.

ACKNOWLEDGMENTS

This research was supported by Matching Grant (Q273) and Industrial Grant (M115) and facilities provided by the Faculty of Mechanical and Manufacturing Engineering, Universiti Tun Hussein Onn Malaysia. Special thank you to Intec Precision Engineering Sdn. Bhd. and AME Manufacturing Sdn. Bhd. as a research collaborator.

REFERENCES

[1] Lane, J. M., Mait, J. E., Unnanuntana, A., Hirsch, B. P., Shaffer, A. D., & Shonuga, O. A. (2011). Materials in Fracture Fixation. Comprehensive Biomaterials, 6, 219–235. https://doi.org/10.1016/B978-0-08-055294-1.00251-8.

[2] Varshney, D., & Kumar, K. (2021). Application and use of different aluminium alloys with respect to workability, strength and welding parameter optimisation. In Ain Shams Engineering Journal (Vol. 12, Issue 1, pp. 1143–1152). Ain Shams University. https://doi.org/10.1016/j.asej.2020.05.013.

[3] Sunny, K. T., Joseph, J., Mangalathu, G. S., & Mathew, J. (2013). A Review on mechanical & microstructural property evaluation of aluminium 5083 alloy weldment. vol, 3, 119-128.

[4] M. L. Doche, J. J. Rameau, R. Durand, F. Novel-Cattin, (1999). Electrochemical behaviour of aluminium in concentrated NaOH solutions, Corrosion Science, 41, Issue 4, 805-826.

[5] H. Puga, J. Barbosa, D. Soares, F. Silva, S. Ribeiro. (2009). Recycling of aluminium swarf by direct incorporation in aluminium melts. Journal of Materials Processing Technology. 209, Issue 11. 5195-5203.

[6] Remolina, M. J., Velasco, M. A., & Córdoba, E. (2021). Chip experimental analysis approach obtained by micro-end-milling in (Ti-6Al-4 V) titanium alloy and (7075) aluminium alloy. Journal of King Saud University - Engineering Sciences. https://doi.org/10.1016/j.jksues.2021.04.003.

[7] Reena Kumari, P. D., Nayak, J., & Nityananda Shetty, A. (2016). Corrosion behavior of 6061/Al-15 vol. pct. SiC(p) composite and the base alloy in sodium hydroxide solution. Arabian Journal of Chemistry, 9, S1144–S1154. https://doi.org/10.1016/j.arabjc.2011.12.003

[8] Xu, Y., Li, G., Jiang, W., Zhan, J., Yu, Y., & Fan, Z. (2022). Investigation on characteristic and formation mechanism of porosity defects of Al–Li alloys prepared by sand casting. Journal of Materials Research and Technology, 19, 4063–4075. https://doi.org/10.1016/J.JMRT.2022.06.148.

[9] Digby D. Macdonald. (1990). Review of mechanistic analysis by electrochemical impedance spectroscopy. Electrochimica Acta, 35, Issue 10, 1509-1525. https://doi.org/10.1016/0013-4686(90)80005-9.

[10] Yanjie Liu, Zhenyao Wang, Wei Ke. (2014). Study on influence of native oxide and corrosion products on atmospheric corrosion of pure Al. Corrosion Science, 80, 169-176.